Intermetallics 174 (2024) 108462

Contents lists available at ScienceDirect

Intermetallics

journal homepage: www.elsevier.com/locate/intermet

Ultrasonic powder consolidation of metallic glass/Al-6061 composites

Jiahao Wang, Senji Liu, Pengyu Huang, Junsheng Liu, Yu Zhang, Xiong Liang, Sajad Sohrabi **, Jiang Ma *

Shenzhen Key Laboratory of High Performance Nontraditional Manufacturing, College of Mechatronics and Control Engineering, Shenzhen University, Shenzhen, 518060, China

ARTICLE INFO

Keywords:
Metallic glass
Aluminum alloy
Composites
Ultrasonic powder consolidation

ABSTRACT

Traditional powder consolidation methods for fabricating metallic matrix composites often require high temperatures, high pressures, and substantial energy consumption. Therefore, developing new processing technologies that can manufacture composites rapidly, efficiently, and economically is crucial. This study introduces ultrasonic powder consolidation process as a novel strategy for fabricating and tuning metallic glass (MG) and aluminum alloy composites. By optimizing the mass ratios of $Zr_{55}Cu_{30}Ni_5Al_{10}$ (at.%) MG to Al-6061 powders, a diverse range of composites with tailored compressive strength and plasticity was achieved. Mechanical testing showed that increasing the aluminum content improved plasticity while maintaining significant strength. Notably, the composite with a 5:5 mass ratio exhibited the best balance of mechanical properties. Morphological characterizations demonstrated excellent densification and uniformity in the composites, with no visible defects and relative densities ranging from approximately 92 %–99 %. Detailed microstructural analysis revealed the formation of a well-bonded interface with a diffusion layer, confirming the metallurgical bonding was facilitated by ultrasonic vibration. Furthermore, the ultrasonic consolidation process enabled the successful fabrication of complex shapes, such as star and gear components, demonstrating the method's potential for advanced manufacturing. These results show that the ultrasonic powder consolidation process is a viable and efficient approach for producing high-quality MG/Al-6061 composites with enhanced mechanical performance and application versatility.

1. Introduction

Metallic glasses (MGs), also known as amorphous alloys, are out-of-equilibrium metallic materials formed through rapid cooling, which prevents crystallization and results in a disordered atomic arrangement in three-dimensional space [1]. Since their discovery in 1960, MGs have attracted significant attention in materials science due to their unique amorphous structure and exceptional mechanical, physical, and chemical properties [2–11]. Compared to traditional crystalline alloys, MGs exhibit high strength [12], high hardness [13], good electrical conductivity [14,15], corrosion resistance [16,17], wear resistance [18], catalytic activity [19], and superplasticity [20]. These properties make MGs highly valuable in fields such as energy, catalysis, electronics, and aerospace [21–25]. However, MGs suffer from poor plasticity at ambient temperatures due to the shear localization in shear bands, posing a significant barrier to their use as structural materials. One strategy to overcome this limitation is the development of in-situ/ex-situ composite structures by incorporating a ductile secondary phase, thereby balancing strength and ductility in MG composites [26].

Aluminum alloys, known for being lightweight and high-strength, exhibit excellent processability, ductility, and corrosion resistance, making them widely used in various industries and daily life applications [27–31]. These desirable properties make them ideal for aerospace [32], automotive manufacturing [33], construction [34], and electronic devices [35]. Due to their good processability and ductility, aluminum alloys can undergo significant deformation without breaking during processing [36,37]. When comparing MGs and aluminum alloys, MGs offer higher strength and hardness, whereas aluminum alloys provide superior processability and ductility. To better suit engineering applications, composites made from rigid MGs and ductile aluminum alloys can combine the advantages of both, compensating for the deficiencies of each material.

* Corresponding author.
** Corresponding author.
E-mail addresses: ssohrabi@szu.edu.cn (S. Sohrabi), majiang@szu.edu.cn (J. Ma).

https://doi.org/10.1016/j.intermet.2024.108462
Received 9 July 2024; Received in revised form 12 August 2024; Accepted 19 August 2024
Available online 26 August 2024

Developing novel processing technologies for rapid, efficient, and cost-effective manufacturing of composites is crucial. Traditional methods for consolidating metal powders to fabricate composites, such as powder metallurgy [38] and spray forming [39], require high temperature, high pressure, high energy consumption, high costs, and often suffer from low efficiency. Recently, a process utilizing ultrasonic vibration to assist in the forming of MGs has been reported [11,40,41]. This method provides an ideal approach for preparing MG/Al composites. Compared to traditional powder consolidation methods, ultrasonic powder consolidation is fast, efficient, clean, and energy-efficient. The mechanism of ultrasonic powder consolidation involves using high-frequency ultrasonic waves to induce softening behavior and plastic flow in both the amorphous alloy and aluminum alloy in a very short time, allowing them to coat each other and form the final composite material.

In this study, biphasic composites of $Zr_{55}Cu_{30}Ni_5Al_{10}$ (at.%) and Al-6061 alloys were successfully fabricated at low temperatures and low stresses using ultrasonic powder consolidation. By adjusting the mass ratio of MG to Al-6061 powder, the properties of the composites could be controlled to obtain materials with comprehensive mechanical properties. This innovative approach offers a promising avenue for the development of high-performance lightweight composites to meet, the demands of advanced manufacturing applications.

2. Experimental procedures

2.1. Material preparation

The MG powder used in this study had a nominal composition of $Zr_{55}Cu_{30}Ni_5Al_{10}$ (at.%), chosen for its high strength (~1.7 GPa), commercial availability, and ability to undergo ultrasonic-vibration-induced plasticity. The gas-atomized MG powder had a particle size range of 15–53 μm with a mass median particle diameter of 35 μm, measured using a laser diffraction system (Malvern, Mastersizer 2000). Gas-atomized Al-6061 powder (300 mesh) was selected as the secondary constituent for the composite due to their cost-effectiveness and high ductility. The composition of Al-6061 powder is provided in Table 1. Both the $Zr_{55}Cu_{30}Ni_5Al_{10}$ MG powder and the Al-6061 powder were purchased commercially. The powders were mixed in various mass ratios of 9:1, 8:2, 7:3, 6:4, 5:5, and 4:6 using a planetary ball mill (ME-300U, Marath industrial, Hong Kong) with hardened steel vials and balls.

2.2. Ultrasonic powder consolidation process

The powder consolidation was carried out using a custom-built ultrasonic vibration setup consisting of a transducer, booster, and ultrasonic horn connected to a control unit to adjust processing parameters (Fig. 1a). The ultrasonic consolidation process is illustrated in Fig. 1b. Initially, the well-mixed powders were loaded into a designated stainless-steel mold with a cavity of Ø5 × 4 mm and compacted using a preset force (100 N) applied by the horn without ultrasonic vibrations. High-frequency ultrasonic vibrations (~20,000 Hz) with an energy of 1500 J were then applied for a few seconds, resulting in consolidated disks.

A K-type thermocouple monitored the temperature rise on the struck surface, while a dynamometer measured the real-time force during ultrasonic vibration loading. Force data was collected using a data-acquisition card (National Instruments NI-9237) with a sampling frequency of 500 Hz. Additionally, composites with a MG/Al-6061 mass ratio of 5:5 were consolidated into star-shaped and gear-shaped stainless-steel molds to investigate the feasibility of manufacturing components of various shapes using ultrasonic powder consolidation.

2.3. Characterizations

The structures of the gas-atomized MG and Al-6061 powders and consolidated composites were analyzed using X-ray diffraction (XRD, Rigaku MiniFlex600) with Cu-K_α radiation. XRD measurements were conducted over an angular range of 20°–80° at a scan rate of 5°/min and a step size of 0.02°. Scanning electron microscopy (SEM, Fei quanta FEG 450) was used to analyze the bonding quality, distribution of constituent powders of consolidated composites as well as the fracture morphology of compressed composites during compression test. Transmission electron microscopy (TEM, JEOL JEM-2011F, 200 kV) equipped with energy-dispersive X-ray spectroscopy (EDS) was used to investigate the microstructure and perform elemental mapping in manufactured composites with a 5:5 ratio of MG to Al-6061. TEM samples were ion milled at 4.5 keV with liquid nitrogen cooling using a precision ion polishing system (Gatan PIPS II). The TEM sampling focused on the interface between the MG powder and Al-6061 powder. EDS analysis was carried out in scanning mode (STEM) using a high-angle annular dark-field (HAADF) detector.

Internal defects in the manufactured composites were characterized using a computed tomography (CT) system (Sanying Precision Instruments-nano Voxel 3000d, China). Uniaxial compression tests were conducted on the composites using a universal testing machine (UTM5105GD) at a strain rate of 10^{-4} s^{-1}. Compression test samples were cuboid samples measuring 1 × 2 × 3 mm^3, wire cut from the consolidated disks. For comparison, compression tests were also performed on samples cut from the as-cast $Zr_{55}Cu_{30}Ni_5Al_{10}$ bulk MG and Al-6061 sheets. The as-cast Zr-based sheet was prepared by suction casting in a water-cooled copper mold. Each condition was tested with three samples to ensure reproducibility. In addition, the hardness of the as-cast MG sheet, Al-6061 sheet, and MG/Al-6061 consolidated composites was measured using a Vickers microhardness tester (FM-ARS9000, Japan) with a static load of 1000 g, a dwell time of 15 s, and making at least 15 measurements per data point. Prior to hardness measurements, the specimen surfaces were polished to a mirror finish.

3. Results and discussion

3.1. Consolidated composites

MG/Al-6061 composites were successfully fabricated using the ultrasonic powder consolidation process. The inset in Fig. 1a shows a Ø5 × 1.2 mm composite disk obtained by consolidating MG and Al-6061 powders with a mass ratio of 5:5. The resulting bulk composite is as consolidated disk with a distinct metallic luster.

The pressure and temperature profiles during ultrasonic powder consolidation for this disk are shown in Fig. 1c. As seen in Fig. 1c, the pressure applied to the composite during the ultrasonic process is only 11.53 MPa, which is significantly lower than the yield stress of $Zr_{55}Cu_{30}Ni_5Al_{10}$ MG (~1700 MPa) and Al-6061 aluminum alloy (~110 MPa). Moreover, the processing time is quite short (~1.2 s), which is considerably shorter than conventional consolidation processes including spark plasma sintering (SPS) and hot pressing of MG components [11]. Fig. 1c also shows that the maximum temperature rise during the ultrasonic process is as low as 183.5 °C, significantly is far below the glass transition temperature of the $Zr_{55}Cu_{30}Ni_5Al_{10}$ MG, which is in the

Table 1
Chemical composition of the Al-6061 powder.

Element	Cu	Mn	Mg	Zn	Cr	Ti	Si	Fe	Al
wt.%	0.15–0.4	0.15	0.8–1.2	0.25	0.04–0.35	0.15	0.4–0.8	0.7	Bal.

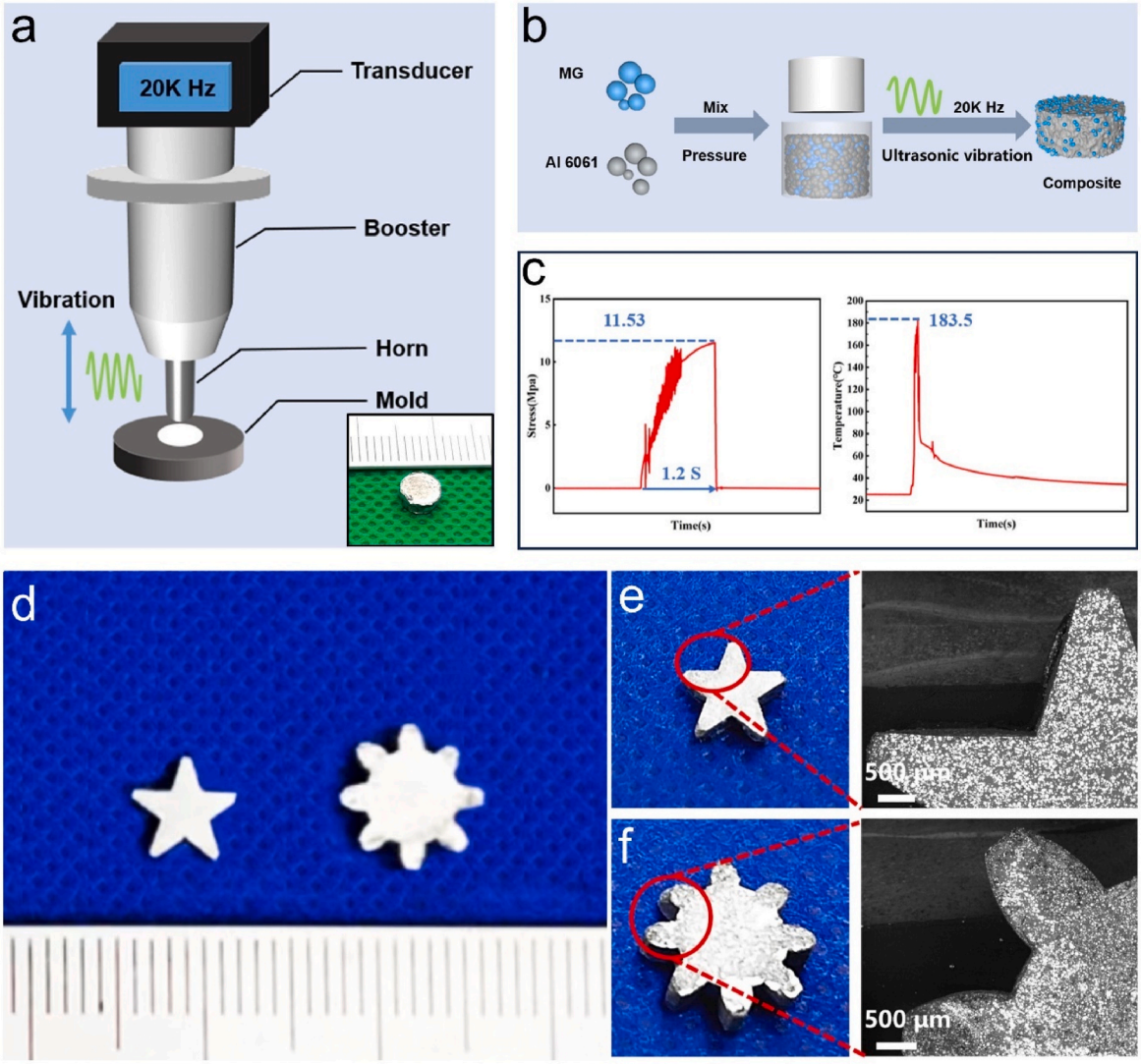

Fig. 1. Ultrasonic consolidation process. (a) Schematic of the apparatus for preparing MG/Al-6061 composites, with an inset showing a consolidated disk. (b) Schematic of the process steps for preparing MG/Al-6061 composites. (c) Pressure and temperature profiles during the ultrasonic process. (d) Overall view of the manufactured composite components in the shapes of a pentagon and a gear. (e–f) SEM images of the pentagon and gear parts.

range of ~407–417 °C [42,43].

These measurements highlight the advantages of using ultrasonic powder consolidation technology to fabricate MG/Al-6061 composites over conventional consolidation methods. The ultrasonic powder consolidation method can rapidly produce intact composite bulk materials at low temperatures and low stresses, demonstrating its efficiency and effectiveness.

Star- and gear-shaped parts were successfully fabricated using ultrasonic consolidation of MG/Al-6061 powders with 5:5 mass ratio (see Fig. 1d). The SEM images in Fig. 1e and f shows that the overall quality of manufactured parts is excellent, with well-formed gear teeth and star vertices and edges. This high quality is attributed to the efficient powder flow during the ultrasonic powder consolidation process and the complete filling of the mold cavities. These results, consistent with previous reports on the successful fabrication of high-entropy alloy and La-based MG composites using ultrasonic vibrations [44], highlight the strong potential of the powder consolidation approach for bonding MG powders across various compositional systems with a broad range of alloy powders.

3.2. Structure and morphology characterizations

Fig. 2a shows the XRD patterns of the $Zr_{55}Cu_{30}Ni_5Al_{10}$ MG powder, Al-6061 powder, and respective MG/Al-6061 consolidated composites with various mass ratios. The insets provide enlarged views of the amorphous peak. The XRD patterns reveal that all composite ratios exhibit broad amorphous peaks alongside sharp crystalline peaks. As the proportion of MG in the composite increases, the intensity of the amorphous peak also rises, confirming that the amorphous structure of the MG remains unchanged after ultrasonic vibration. Furthermore, the intensity of the crystalline peaks correlates positively with the ratio of Al-6061 powder in the composite.

Fig. 2b–g displays the SEM cross-sectional morphologies of composites with different mass ratios after ultrasonic consolidation. In the images, the dark regions correspond to the aluminum alloy matrix, while the bright regions represent the MG component of the composite. The SEM images of different samples reveal good densification with no apparent pores or cracks, indicating a high-quality bond in all consolidated composites.

During the ultrasonic consolidation process, an interesting phenomenon was observed. As shown in Fig. 2b, when the composite has a high MG content with a MG/Al-6061 mass ratio of 9:1, both the MG

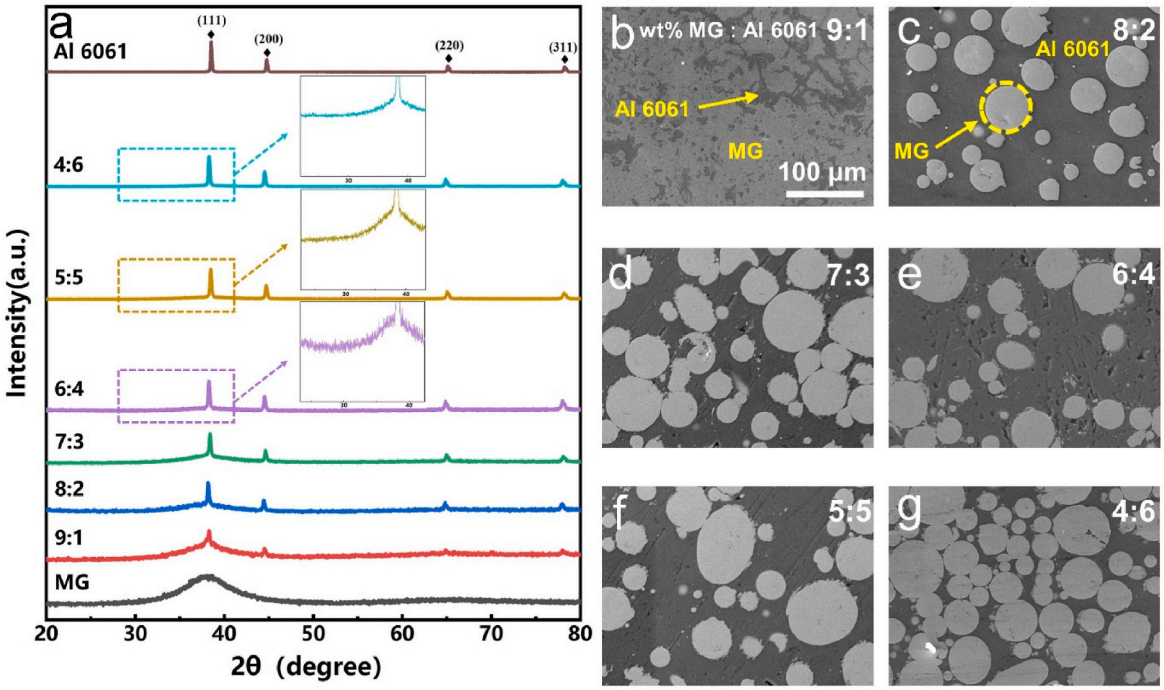

Fig. 2. (a) XRD patterns of MG powder, Al-6061 powder, and consolidated composites with various ratios. The inset shows an enlarged view of the amorphous peak. (b)–(g) SEM cross-sectional images of composites with amorphous alloy to aluminum alloy mass ratios of 9:1, 8:2, 7:3, 6:4, 5:5, and 4:6, respectively.

(bright regions) and Al-6061 (dark regions) powders undergo softening and plastic flow, resulting in bonding and forming the bulk sample. This morphology, featuring a continuous distribution of both phases, is uncommon in ex-situ MG composites and resembles the morphology of in-situ MG matrix composites [26].

However, as the MG proportion decreases, the MG powder keeps its

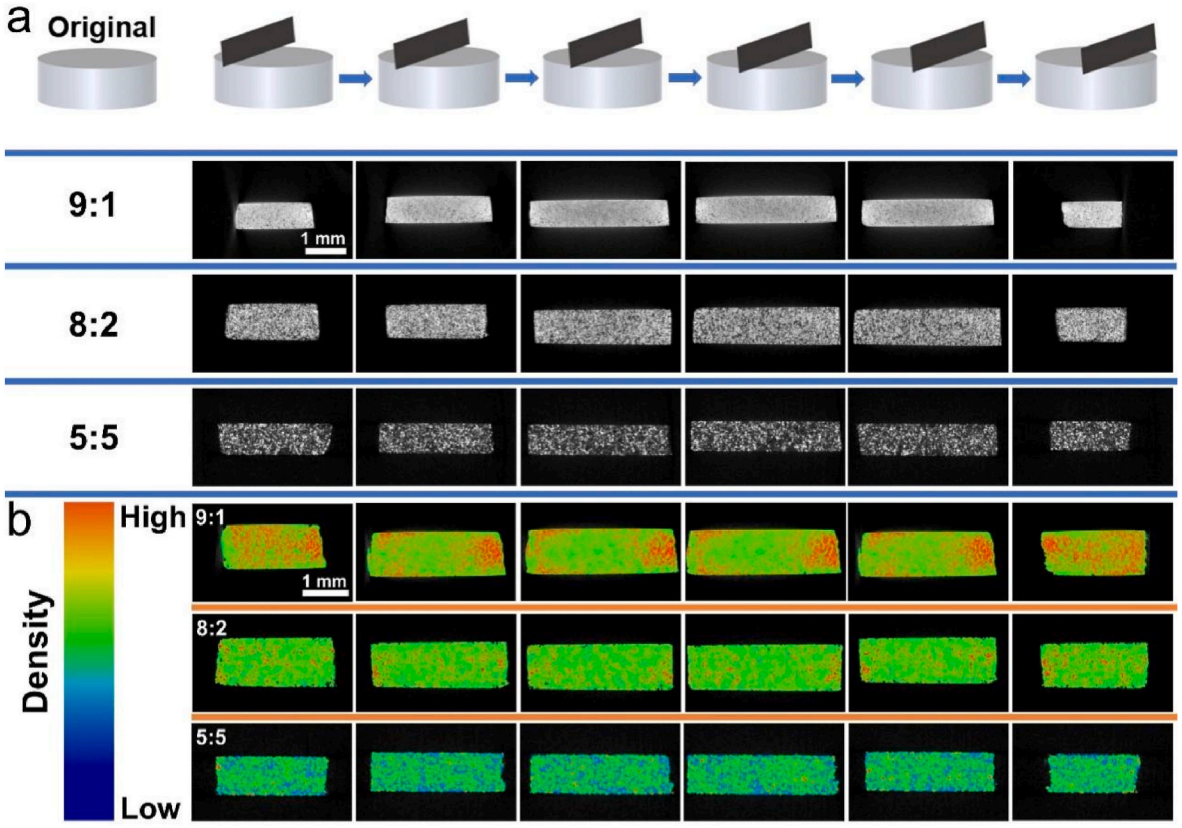

Fig. 3. CT scan images. (a) Cross-sectional CT images at different cutting positions from the edge to the center, with the inset showing the cutting positions of the samples. (b) Density distribution map of the composite samples.

round shape and does not further show ultrasonic vibration-induced plasticity, whereas the aluminum alloy continues to show softening and plastic flow. Thus, Al-6061 acts as the matrix, encapsulating the MG powders. This morphology is typical in ex-situ MG composites and has been observed in the ultrasonic powder consolidation of MG/high-entropy alloys [44]. Given the lower yield stress and hardness of Al-6061 compared to that of the Zr-based MG in this study, the aluminum alloy powders dissipate most of the ultrasonic energy through plastic flow, forming a composite matrix that surrounds the rigid MG powder. Furthermore, the SEM images in Fig. 2c–g reveal that the bonding between the Al-6061 and MG powders in the composites is stable, with well-bonded interfaces formed by ultrasonic powder consolidation.

3.3. CT analysis

High-resolution CT analysis was employed to scan the composites, providing a clear display of the internal structure and enabling the detection of uniformity and potential defects within the samples. Three representative composites with MG:Al-6061 mass ratios of 9:1, 8:2, and 5:5 were selected for scanning at different cutting positions from the edge to the center, as illustrated in Fig. 3a. The CT images reveal the internal structure of the composites, showing uniform bonding between the amorphous alloy and aluminum alloy with no visible defects. To further illustrate the bonding of the two different phase metal powders, the CT images of the samples were presented as relative density ($\rho_{relative}$) distribution maps, as shown in Fig. 3b. These maps indicate that the density distribution of the composites is relatively uniform. Additionally, the overall sample density decreases as the proportion of aluminum alloy in the composite increases. This is attributed to the lower density of Al-6061 lightweight alloy compared to the $Zr_{55}Cu_{30}Ni_5Al_{10}$ MG.

In addition to CT scanning, density is an important indicator of the bonding quality of composites. The densities of the MG sheet, Al-6061 sheet, and consolidated composites were measured using the Archimedes drainage method. The measured densities were then compared with theoretical densities. The actual densities of the MG, Al-6061, and composites were calculated using the following equation:

$$\rho_{actual} = (\omega_1 \times \rho_1) / (\omega_1 - \omega_2) \quad (1)$$

where ρ_{actual} represents the actual density of the object, ρ_1 represents the density of distilled water at room temperature (0.999 g/cm^3), and ω_1、ω_2 represent the weights of the object in air and distilled water, respectively.

Repeated measurements using this equation yielded average densities of 5.643 g/cm^3 for the as-cast MG sheet and 2.649 g/cm^3 for the Al-6061 sheet. Furthermore, the theoretical density of the composite materials was calculated using the following equation:

$$\rho_{theoretical} = \frac{(\omega_{MG} + \omega_{admixture})}{(\omega_{MG}/\rho_{MG} + \omega_{admixture}/\rho_{admixture})} \quad (2)$$

Using equations (1) and (2), the average actual and theoretical densities for composites with mass ratios of MG to aluminum alloy of 9:1, 8:2, 7:3, 6:4, 5:5, and 4:6 were calculated, as shown in Table 2.

Comparing the actual and theoretical densities of the composites in Table 2, it can be seen that the actual densities of the composites are close to their theoretical densities, with a minimum correlation density of over 92 %. These results indicate that the ultrasonic powder consolidation method is a feasible and efficient way to fabricate MG and aluminum alloy composites.

Table 2
Density comparison of composites with different mass ratios.

mass ratio (wt.%)	ρ_{actual} (g/cm^3)	$\rho_{theoretical}$ (g/cm^3)	$\rho_{relative}$ (%)
9:1	5.643	5.729	98.50
8:2	4.875	5.074	96.08
7:3	4.217	4.553	92.62
6:4	3.876	4.129	93.87
5:5	3.515	3.777	93.06
4:6	3.263	3.481	93.74

3.4. Mechanical property characterizations

Fig. 4a shows the compressive stress-strain curves for the consolidated MG/Al-6061 samples, along with the Al-6061 bulk sample. The inset displays the stress-strain curve of the cast bulk MG sample during the compression testing. The Al-6061 alloy exhibits the lowest compressive strength, around 110 MPa, but shows the best plasticity. In contrast, the cast MG sample demonstrates a high compressive strength of approximately 1700 MPa, but with no plasticity, which is characteristic of monolithic bulk MGs [45]. As the aluminum alloy content in the consolidated composites increases, the composite's strength gradually decreases, but its plasticity significantly improves. The composite benefits from the advantageous properties of both constituting materials, achieving a notable increase in strength compared to Al-6061 and a considerable improvement in plasticity compared to the MG. Among the various consolidated composites, the composite with a MG:Al-6061 mass ratio of 5:5 exhibits the best mechanical performance.

Additionally, the Vickers hardness testing was conducted on the bulk MG and Al-6061 alloys and the consolidated composites. The results, shown in Fig. 4b, indicate that the Zr-based MG has the highest hardness, while the Al-6061 has the lowest. The hardness of the composites falls between the two constituent materials and decreases with increasing Al-6061 content due to the relatively soft nature of aluminum alloy.

Fig. 4c shows the fracture morphology of the 5:5 composite after the compression test. The fracture surface reveals that the spherical MG powders remain undeformed, while the Al-6061 matrix undergoes complete plastic deformation, indicating ductile behavior in the 5:5 composite. Additionally, a few voids are observed on the fractured surface, but these voids are discontinuous and have a low number-density. This suggests that MG particles are not responsible for the composite's failure under compression. The SEM image at higher magnification (Fig. 4d) reveals the presence of dimples on the fracture surface. It can be inferred from the fracture morphology that the primary failure mechanism is the crack propagation around the MG powder, leading to the detachment of the MG particles from the surrounding Al-6061 matrix.

3.5. TEM characterizations

To further investigate the microstructure of the composite achieved by ultrasonic consolidation, we performed TEM analysis on the 5:5 composite, focusing primarily on the interface between the MG powder and Al-6061 powder. The TEM images of the interface region are shown in Fig. 5a and b. These images reveal three distinct regions, denoted as R1, R2, and R3 (Fig. 5b). The corresponding selected area electron diffraction (SAED) patterns for these regions are displayed in Fig. 5c, d, and e, respectively.

In Fig. 5c, the SAED pattern of the R1 region displays a diffuse halo ring typical of amorphous structures, indicating that this region is a fully amorphous phase and that the amorphous structure was retained after ultrasonic vibration loading. In the R2 region, located at the interface of MG/Al-6061 powders, the diffraction pattern exhibits a combination of diffuse halo ring and crystalline diffraction spots (Fig. 5d), indicating that this region consists of a mixture of MG amorphous phase and Al-6061 crystalline phase. In the R3 region, the diffraction halo disappears, leaving only diffraction spots (Fig. 5e), indicating that this region is a fully aluminum alloy phase.

Additionally, the high-resolution TEM images taken from the R1 and R3 regions show maze structure (fully amorphous) and regular lattice fringe contrast (crystalline structure), respectively. However, the R2

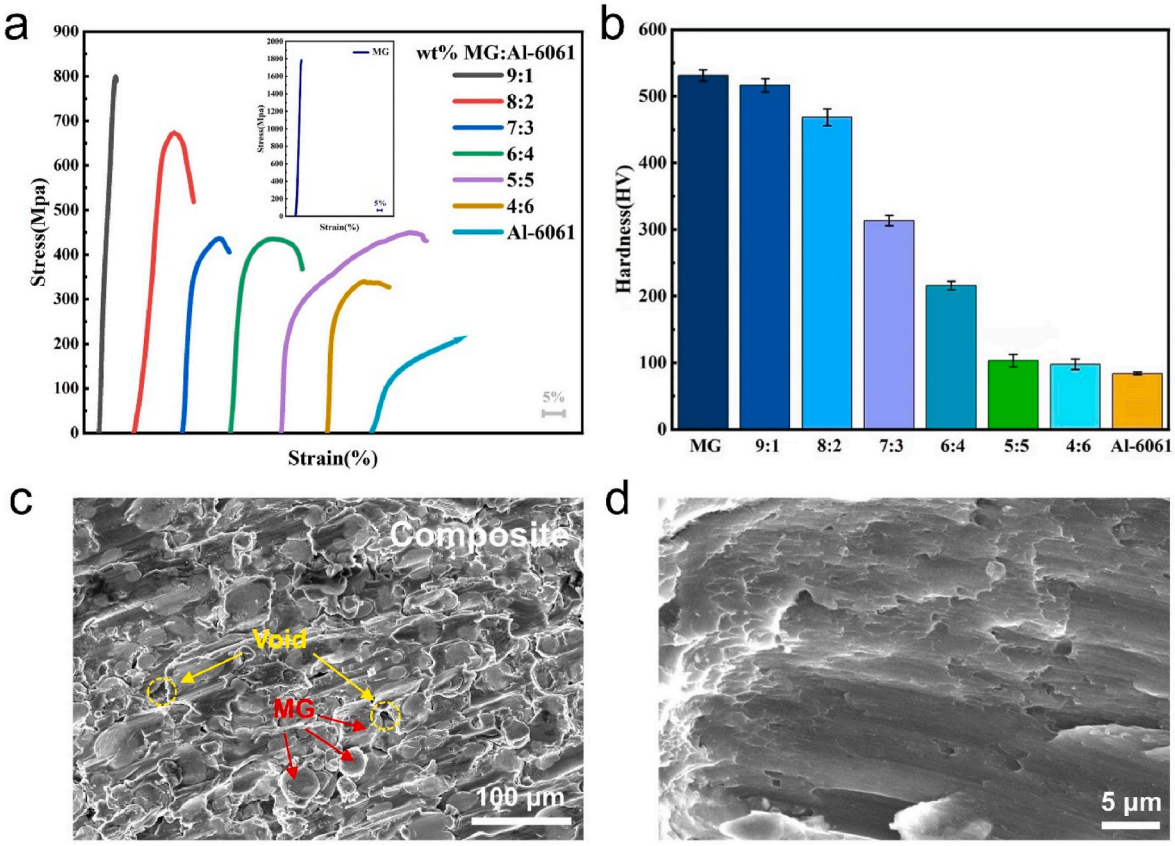

Fig. 4. (a) Compressive stress-strain curves of bulk MG, bulk Al-6061 alloy, and consolidated composite samples with various ratios. (b) Vickers hardness test results for the bulk MG, bulk Al-6061 alloy, and consolidated composite samples with various ratios. (c) The SEM image of the fracture surface of a 5:5 composite sample. (d) The SEM image of the fracture surface at higher magnification.

interface region contains both features (Fig. 5f, g, and h). The gradual changes in the diffraction patterns and microstructure of these three regions reflects the binary phase composition of the consolidate composite [44].

Furthermore, we employed EDS analysis to characterize elemental distribution of the 5:5 composite across the MG/Al-6061 bonding interface. The HAADF-STEM image of the interface region and corresponding EDS maps are shown in Fig. 5i. The bright contrast region in the HAADF-STEM image is rich in Zr, which corresponds to the $Zr_{55}Cu_{30}Ni_5Al_{10}$ MG, while the dark contrast region is rich in Al, corresponding to the Al-6061 alloy. Observing the elemental distribution at the micro-region of the interface reveals mutual diffusion of chemical elements across the interface, indicating the existence of metallurgical bonding between MG and aluminum alloy due to the interdiffusion of elements [46]. According to Fig. 5g, the diffusion layer at the interface has a thickness of ~5 nm. This value is comparable to the thickness of the diffusion layer observed in La-based MG/high-entropy alloy (5:5) composite fabricated by the same ultrasonic powder consolidation approach [44], suggesting that the diffusion layer is primarily influenced by the ultrasonic processing parameters rather than the chemical composition of the composite's constituent phases.

3.6. Bonding mechanism

Dense oxide layers typically act as barriers to bonding in metals. Therefore, breaking through these oxide layers is essential to enable better bonding in MGs [47]. The ultrasonic vibration loading is a well-recognized approach to rupturing the oxide layer, enhancing the atomic diffusion, inducing plastic flow, and contributing significantly to the stable bonding of MGs with other metals [46,48].

Under the high-frequency ultrasonic vibration used in this study, the oxide layers on MG and Al-6061 are disrupted, facilitating element transfer. As shown in Fig. 5g and a, some elements interdiffuse near the interface, forming a diffusion layer that promotes bonding between the MG and Al-6061. Additionally, the plastic flow exhibited by the MG and Al-6061 alloy under ultrasonic vibration further contributes to the bonding. From Fig. 2b–g, it is evident that under ultrasonic vibration loading, when the mass ratio of MG to Al-6061 is 9:1, both phases undergo plastic flow, causing MG and Al-6061 to act like glue [49] and bond together effectively, resulting in a dense composite material. For other composite ratios, the ultrasonic vibration-induced plasticity occurs primarily in the Al-6061 alloy, forming composites where the aluminum alloy acts as the matrix, tightly encapsulating MG particles.

Overall, our results highlight that the ultrasonic powder consolidation approach offers several key advantages: it operates at low temperatures and under low stress, utilizes clean energy, and is both convenient and rapid. Moreover, the mechanical properties of the resulting composites can be readily tailored by adjusting the mass ratio of the constituent materials. Additionally, this technique shows potential for bonding MGs with other functional materials, enabling the development of composite materials with enhanced mechanical, magnetic and electrical properties for diverse engineering applications.

4. Conclusion

Composites of $Zr_{55}Cu_{30}Ni_5Al_{10}$ MG and Al-6061 are successfully fabricated using the ultrasonic powder consolidation method, operating under low temperature and low stress conditions. By adjusting the mass ratios of amorphous alloy and Al-6061, the compressive strength and plasticity of the composites are controlled effectively. Excellent bonding

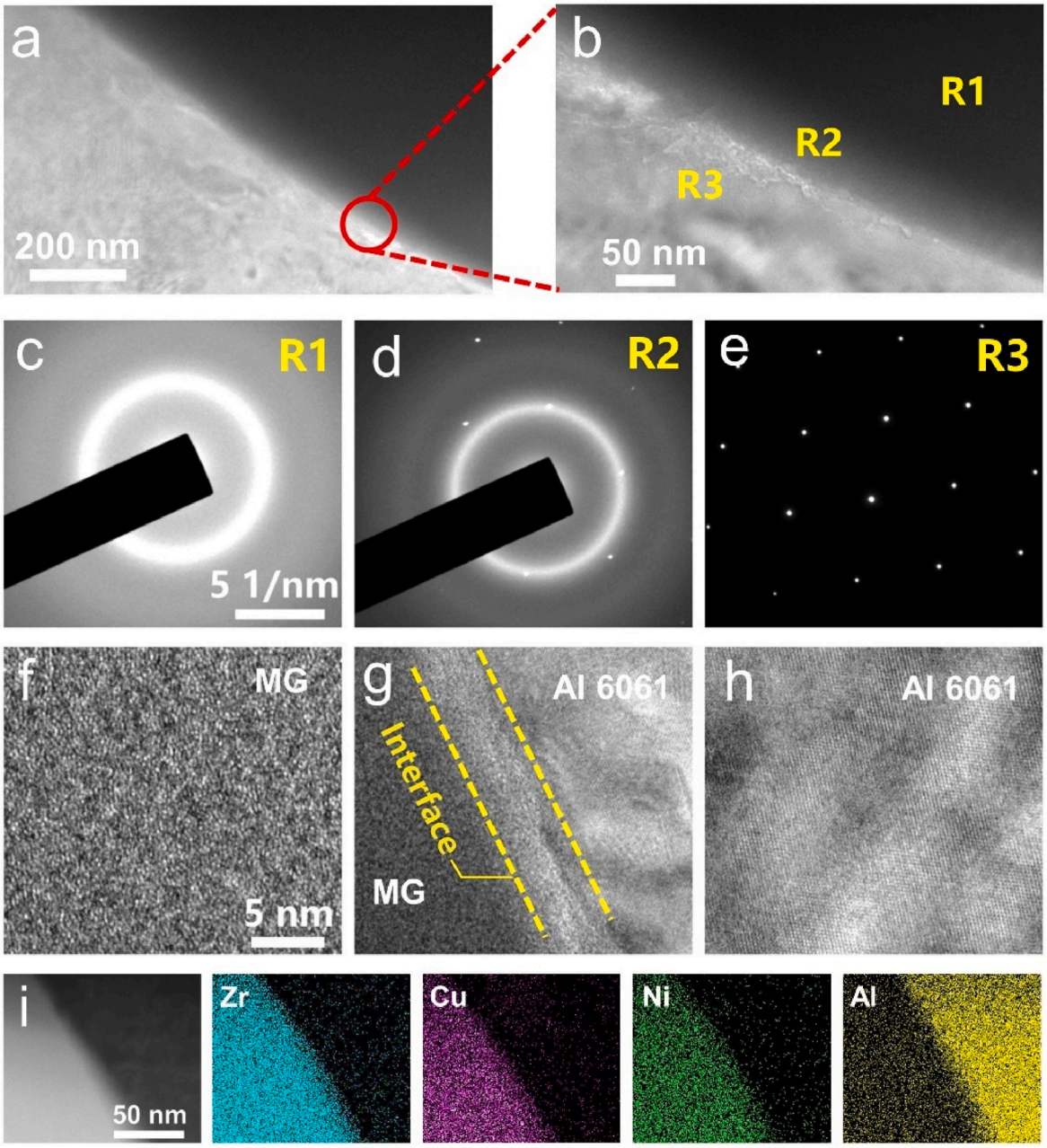

Fig. 5. (a) The TEM image at the bonding interface. (b) The local enlarged image of (a). (c–e) The diffraction patterns corresponding to regions R1, R2, and R3 in (b). (f–h) The high-resolution TEM images from regions R1, R2, and R3 in (b). (i) The HAADF-STEM image of the bonding interface and EDS elemental distribution in the microscopic region of the bonding interface.

quality, with no observable pores or cracks, is confirmed through microscopic observations and CT analysis. The composite structure, combining soft Al-6061 phase and Zr-based rigid phase, enhances overall mechanical properties compared to single-phase materials. Our findings introduce a novel processing method and design principles for manufacturing MG/Al-6061 composite materials tailored to specific mechanical performance requirements.

CRediT authorship contribution statement

Jiahao Wang: Writing – review & editing, Writing – original draft, Methodology, Investigation, Formal analysis, Data curation. **Senji Liu:** Methodology, Investigation. **Pengyu Huang:** Methodology, Investigation, Data curation. **Junsheng Liu:** Investigation, Formal analysis, Conceptualization. **Yu Zhang:** Methodology, Formal analysis, Data curation. **Xiong Liang:** Supervision, Resources, Project administration. **Sajad Sohrabi:** Writing – review & editing, Writing – original draft, Supervision, Methodology, Conceptualization. **Jiang Ma:** Writing – review & editing, Supervision, Resources, Project administration, Funding acquisition.

Declaration of competing interest

The authors declare that they have no known competing financial interests or personal relationships that could have appeared to influence the work reported in this paper.

Data availability

Data will be made available on request.

Acknowledgments

The work was financially supported by the Key Basic and Applied Research Program of Guangdong Province, China (Grant No. 2019B030302010), the NSF of China (Grant No. 52122105, 52271150), and the Science and Technology Innovation Commission Shenzhen (Grants No. RCJC20221008092730037, 20220804091920001). The authors also thank the assistance on microscope observation received from the Electron Microscope Center of Shenzhen University.

References

[1] M. Ashby, A. Greer, Metallic glasses as structural materials, Scripta Mater. 54 (3) (2006) 321–326.
[2] F. Bridges, T. Keiber, P. Juhas, S.J.L. Billinge, L. Sutton, J. Wilde, G.R. Kowach, Local vibrations and negative thermal expansion in ZrW2O8, physical review letters, Am. Phys. Soc. (2014) 045505.
[3] J.-L. Barrat, J.J. de Pablo, Modeling deformation and flow of disordered materials, MRS Bull. 32 (11) (2007) 941–944.
[4] A. Inoue, A. Takeuchi, Recent development and application products of bulk glassy alloys, Acta Mater. 59 (6) (2011) 2243–2267.
[5] H. Jiang, T. Shang, H. Xian, B. Sun, Q. Zhang, Q. Yu, H. Bai, L. Gu, W. Wang, Structures and functional properties of amorphous alloys, Small Struct. 2 (2) (2020).
[6] H. Zhao, F. Sun, X. Li, Y. Ding, Y.Q. Yan, X. Tong, J. Ma, H.B. Ke, W.H. Wang, Ultrastability of metallic supercooled liquid induced by vibration, Scripta Mater. 194 (2021) 113606.
[7] B. Lin, X. Bian, P. Wang, G. Luo, Application of Fe-based metallic glasses in wastewater treatment, Mater. Sci. Eng., B 177 (1) (2012) 92–95.
[8] J.C. Qiao, Q. Wang, J.M. Pelletier, H. Kato, R. Casalini, D. Crespo, E. Pineda, Y. Yao, Y. Yang, Structural heterogeneities and mechanical behavior of amorphous alloys, Prog. Mater. Sci. 104 (2019) 250–329.
[9] J. Schroers, Processing of bulk metallic glass, Adv. Mater. 22 (14) (2010) 1566–1597.
[10] C. Schuh, T. Hufnagel, U. Ramamurty, Mechanical behavior of amorphous alloys, Acta Mater. 55 (12) (2007) 4067–4109.
[11] S. Sohrabi, J. Fu, L. Li, Y. Zhang, X. Li, F. Sun, J. Ma, W.H. Wang, Manufacturing of metallic glass components: processes, structures and properties, Prog. Mater. Sci. 144 (2024) 101283.
[12] F.-F. Wu, K.C. Chan, S.-S. Jiang, S.-H. Chen, G. Wang, Bulk metallic glass composite with good tensile ductility, high strength and large elastic strain limit, Sci. Rep. 4 (1) (2014).
[13] R.L. Narayan, K. Boopathy, I. Sen, D.C. Hofmann, U. Ramamurty, On the hardness and elastic modulus of bulk metallic glass matrix composites, Scripta Mater. 63 (7) (2010) 768–771.
[14] W. Bao, L. Bao, J. Chen, J. Li, T. Xiang, B. Yu, Z. Cai, G. Xie, Heterogeneous metallic glass composites with a unique combination of strength, plasticity and conductivity, Int. J. Plast. 171 (2023).
[15] M. Yamasaki, S. Kagao, Y. Kawamura, Thermal diffusivity and conductivity of Zr55Al10Ni5Cu30 bulk metallic glass, Scripta Mater. 53 (1) (2005) 63–67.
[16] T.C. Chieh, J. Chu, C.T. Liu, J.K. Wu, Corrosion of Zr52.5Cu17.9Ni14.6Al10Ti5 bulk metallic glasses in aqueous solutions, Mater. Lett. 57 (20) (2003) 3022–3025.
[17] Q. Jing, B. Zhang, J. Zhang, M. Ma, R. Liu, Electrochemical corrosion and oxidation resistances of Zr60Ni21Al19 bulk amorphous alloys, Sci. China Phys. Mech. Astron. 53 (12) (2010) 2223–2226.
[18] R.C.Y. Tam, C.H. Shek, Abrasion resistance of Cu based bulk metallic glasses, J. Non-Cryst. Solids 347 (1–3) (2004) 268–272.
[19] Z. Jia, X. Duan, P. Qin, W. Zhang, W. Wang, C. Yang, H. Sun, S. Wang, L.C. Zhang, Disordered atomic packing structure of metallic glass: toward ultrafast hydroxyl radicals production rate and strong electron transfer ability in catalytic performance, Adv. Funct. Mater. 27 (38) (2017).
[20] J. Ma, X. Liang, X. Wu, Z. Liu, F. Gong, Sub-second thermoplastic forming of bulk metallic glasses by ultrasonic beating, Sci. Rep. 5 (1) (2015).
[21] Z. Deng, C. Zhang, L. Liu, Chemically dealloyed MgCuGd metallic glass with enhanced catalytic activity in degradation of phenol, Intermetallics 52 (2014) 9–14.
[22] R. Hasegawa, D. Azuma, Impacts of amorphous metal-based transformers on energy efficiency and environment, J. Magn. Magn Mater. 320 (20) (2008) 2451–2456.
[23] S.Y. Kim, M.H. Lee, T.S. Kim, B.S. Kim, Co oxidation properties of selective dissoluted metallic glass composites, Arch. Metall. Mater. 60 (2) (2015) 1227–1229.
[24] H. Liu, J. Li, J. Zhang, P. Gong, W. Yang, L. Zhao, X. Wang, Design optimization and mechanical properties of SiC particle reinforced Ti-based metallic glass matrix composite, Materials 16 (15) (2023).
[25] E. Sharifikolouei, A. Żywczak, B. Sarac, T. Koziel, R. Rashidi, P. Bala, M. Fracasso, R. Gerbaldo, G. Ghigo, L. Gozzelino, D. Torsello, Soft magnetic properties and electromagnetic shielding performance of Fe40Ni40B20 microfibers, Adv. Electr. Mater. 9 (8) (2023).
[26] J. Qiao, H. Jia, P.K. Liaw, Metallic glass matrix composites, Mater. Sci. Eng. R Rep. 100 (2016) 1–69.
[27] L. Feng, F. Sultonzoda, J. Wang, H. Wang, F. Xue, Superhydrophobic aluminum alloy surface with excellent universality, corrosion resistance, and antifouling performance prepared without prepolishing, Mater. Corros. 72 (4) (2020) 652–659.
[28] M. Starostin, G.E. Shter, G.S. Grader, Corrosion of aluminum alloys Al 6061 and Al 2024 in ammonium nitrate-urea solution, Mater. Corros. 67 (4) (2015) 387–395.
[29] X.K. Yang, L.W. Zhang, S.Y. Zhang, M. Liu, K. Zhou, X.L. Mu, Properties degradation and atmospheric corrosion mechanism of 6061 aluminum alloy in industrial and marine atmosphere environments, Mater. Corros. 68 (5) (2016) 529–535.
[30] E. Yao, H. Zhang, K. Ma, C. Ai, Q. Gao, X. Lin, Effect of deep cryogenic treatment on microstructures and performances of aluminum alloys: a review, J. Mater. Res. Technol. 26 (2023) 3661–3675.
[31] X. Yu, G. Zhang, Z. Zhang, Y. Wang, Research on corrosion resistance of anodized and sealed 6061 aluminum alloy in 3.5 % sodium chloride solution, Int. J. Electrochem. Sci. 18 (5) (2023).
[32] T. Dursun, C. Soutis, Recent developments in advanced aircraft aluminium alloys, Mater. Des. 56 (2014) 862–871, 1980-2015.
[33] Q. Zhang, M. Cao, D. Zhang, S. Zhang, J. Sun, Research on integrated casting and forging process of aluminum automobile wheel, Adv. Mech. Eng. 6 (2015).
[34] M. Fan, X. Wang, Research on the mechanical properties of some new aluminum alloy composite structures in construction engineering, Korean J. Mater. Res. 34 (2) (2024) 72–78.
[35] M. Sundararajan, M. Devarajan, M. Jaafar, Investigation of surface and mechanical properties of Anodic Aluminium Oxide (AAO) developed on Al substrate for an electronic package enclosure, Surf. Coating. Technol. 401 (2020).
[36] B.Q. Han, T.G. Langdon, Achieving enhanced tensile ductility in an Al-6061 composite processed by severe plastic deformation, Mater. Sci. Eng., A 410–411 (2005) 430–434.
[37] H. Zhu, F. Qi, Mechanical properties and fracture behaviors on 6061 aluminum alloy under shear stress state, Rare Met. 30 (5) (2011) 550–554.
[38] K.B. Jiju, G. Selvakumar, S. Ram Prakash, Study on preparation of Al – SiC metal matrix composites using powder metallurgy technique and its mechanical properties, Mater. Today: Proc. 27 (2020) 1843–1847.
[39] S.K. Chaudhury, C.S. Sivaramakrishnan, S.C. Panigrahi, A new spray forming technique for the preparation of aluminium rutile (TiO2) ex situ particle composite, J. Mater. Process. Technol. 145 (3) (2004) 385–390.
[40] X. Li, D. Wei, J.Y. Zhang, X.D. Liu, Z. Li, T.Y. Wang, Q.F. He, Y.J. Wang, J. Ma, W. H. Wang, Y. Yang, Ultrasonic plasticity of metallic glass near room temperature, Appl. Mater. Today 21 (2020).
[41] X. Li, L. Li, S. Sohrabi, J.n. Fu, Z. Li, Z. Chen, R. Sun, Y. Zhang, J. Huang, H. Zhang, J. Zhu, X. Chen, K. Song, J. Ma, Ultrasonic vibration enabled under-liquid forming of metallic glasses, Sci. Bull. 69 (2) (2024) 163–166.
[42] L. Liu, Z.F. Wu, J. Zhang, Crystallization kinetics of Zr55Cu30Al10Ni5 bulk amorphous alloy, J. Alloys Compd. 339 (1) (2002) 90–95.
[43] S. Sohrabi, R. Gholamipour, Glass transition kinetics and fragility of ZrCuAlNi(Nb) metallic glasses, Intermetallics 145 (2022) 107532.
[44] X. Liang, K. Wu, J. Fu, L. Li, C. Fan, W. Wen, W. Ruan, S. Ren, Z. Zhang, J. Ma, Fabrication of amorphous and high-entropy biphasic composites using high-frequency ultrasonic vibration, J. Non-Cryst. Solids 582 (2022) 121458.
[45] W.H. Wang, C. Dong, C.H. Shek, Bulk metallic glasses, Mater. Sci. Eng. R Rep. 44 (2–3) (2004) 45–89.
[46] L. Li, X. Li, Z. Huang, J. Huang, Z. Liu, J. Fu, W. Wen, Y. Zhang, S. Huang, S. Ren, J. Ma, Joining of metallic glasses in liquid via ultrasonic vibrations, Nat. Commun. 14 (1) (2023) 6305.
[47] W. Chen, Z. Liu, J. Schroers, Joining of bulk metallic glasses in air, Acta Mater. 62 (2014) 49–57.
[48] X. Li, X. Liang, Z. Zhang, J. Ma, J. Shen, Cold joining to fabricate large size metallic glasses by the ultrasonic vibrations, Scripta Mater. 185 (2020) 100–104.
[49] J. Fu, J. Yang, K. Wu, H. Lin, W. Wen, W. Ruan, S. Ren, Z. Zhang, X. Liang, J. Ma, Metallic glue for designing composite materials with tailorable properties, Mater. Horiz. 8 (6) (2021) 1690–1699.